Self-referenced single-shot THz detection

BRANDON K. RUSSELL,[1,2,4] BENJAMIN K. OFORI-OKAI,[1,3,4] ZHIJIANG CHEN,[1] MATTHIAS C. HOFFMANN,[1], YING Y. TSUI,[2] AND SIEGFRIED H. GLENZER[1,*]

[1]*SLAC National Accelerator Laboratory, 2575 Sand Hill Road, Menlo Park, California 94025, USA*
[2]*Department of Electrical and Computer Engineering, University of Alberta, Edmonton, Alberta T6G2V4, Canada*
[3]*Department of Chemistry, Massachusetts Institute of Technology, Cambridge, Massachusetts 02139, USA*
[4]*Contributed equally*
[*]*glenzer@SLAC.stanford.edu*

Abstract: We demonstrate a self-referencing method to reduce noise in a single-shot terahertz detection scheme. By splitting a single terahertz pulse and using a reflective echelon, both the signal and reference terahertz time-domain waveforms were measured using one laser pulse. Simultaneous acquisition of these waveforms significantly reduces noise originating from shot-to-shot fluctuations. We show that correlation function based referencing, which is not limited to polarization dependent measurements, can achieve a noise floor that is comparable to state-of-the-art polarization-gated balanced detection. Lastly, we extract the DC conductivity of a 30 nm free-standing gold film using a single THz pulse. The measured value of $\sigma_0 = 1.3 \pm 0.4 \times 10^7$ S m^{-1} is in good agreement with the value measured by four-point probe, indicating the viability of this method for measuring dynamical changes and small signals.

OCIS codes: (300.6495) Spectroscopy, terahertz; (320.7100) Ultrafast measurements; (320.0320) Ultrafast optics; (040.1880) Detection; (110.0110) Imaging systems; (310.0310) Thin films.

References and links

1. M. Nuss and J. Orenstein, "Terahertz time-domain spectroscopy," in *Millimeter and Submillimeter Wave Spectroscopy of Solids*, G. Grüner, ed. (Springer Berlin Heidelberg, 1998), pp. 7–50.
2. M. C. Beard, G. M. Turner, and C. A. Schmuttenmaer, "Terahertz Spectroscopy," J. Phys. Chem. B **106**(29), 7146–7159 (2002).
3. C. A. Schmuttenmaer, "Exploring dynamics in the far-infrared with terahertz spectroscopy," Chem. Rev. **104**(4), 1759–1779 (2004).
4. R. Ulbricht, E. Hendry, J. Shan, T. F. Heinz, and M. Bonn, "Carrier dynamics in semiconductors studied with time-resolved terahertz spectroscopy," Rev. Mod. Phys. **83**(2), 543–586 (2011).
5. J. Lloyd-Hughes and T.-I. Jeon, "A review of the terahertz conductivity of bulk and nano-materials," J. Infrared, Millimeter, Terahertz Waves **33**(9), 871–925 (2012).
6. D. H. Auston and M. C. Nuss, "Electrooptical generation and detection of femtosecond electrical transients," IEEE J. Quantum Electron. **24**(2), 184–197 (1988).
7. A. Nahata, D. H. Auston, T. F. Heinz, and C. Wu, "Coherent detection of freely propagating terahertz radiation by electro-optic sampling," Appl. Phys. Lett. **68**(2), 150–152 (1996).
8. Q. Wu and X. C. Zhang, "Ultrafast electro-optic field sensors," Appl. Phys. Lett. **68**(12), 1604–1606 (1996).
9. K. Reimann, R. P. Smith, A. M. Weiner, T. Elsaesser, and M. Woerner, "Direct field-resolved detection of terahertz transients with amplitudes of megavolts per centimeter," Opt. Lett. **28**(6), 471–473 (2003).
10. S. M. Teo, B. K. Ofori-Okai, C. A. Werley, and K. A. Nelson, "Invited Article: Single-shot THz detection techniques optimized for multidimensional THz spectroscopy," Rev. Sci. Instrum. **86**(5), 051301 (2015).
11. Z. Jiang and X. C. Zhang, "Single-shot spatiotemporal terahertz field imaging," Opt. Lett. **23**(14), 1114–1116 (1998).
12. N. H. Matlis, G. R. Plateau, J. van Tilborg, and W. P. Leemans, "Single-shot spatiotemporal measurements of ultrashort THz waveforms using temporal electric-field cross correlation," J. Opt. Soc. Am. B **28**(1), 23–27 (2011).
13. X. Wang, Y. Fei, and L. Li, "Detection of the spatiotemporal field of a single-shot terahertz pulse based on spectral holography," Chinese Phys. B **23**(6), 064202 (2014).
14. J. Shan, A. S. Weling, E. Knoesel, L. Bartels, M. Bonn, A. Nahata, G. A. Reider, and T. F. Heinz, "Single-shot measurement of terahertz electromagnetic pulses by use of electro-optic sampling," Opt. Lett. **25**(6), 426–428 (2000).

This material is based upon work supported by the U.S. Department of Energy, Office of Science, under Contract No. DE-AC02-76SF00515.

15. S. P. Jamison, J. Shen, A. M. MacLeod, W. A. Gillespie, and D. A. Jaroszynski, "High-temporal-resolution, single-shot characterization of terahertz pulses," Opt. Lett. **28**(18), 1710–1712 (2003).
16. K. Y. Kim, B. Yellampalle, A. J. Taylor, G. Rodriguez, and J. H. Glownia, "Single-shot terahertz pulse characterization via two-dimensional electro-optic imaging with dual echelons," Opt. Lett. **32**(14), 1968–1970 (2007).
17. Y. Kawada, T. Yasuda, A. Nakanishi, K. Akiyama, and H. Takahashi, "Single-shot terahertz spectroscopy using pulse-front tilting of an ultra-short probe pulse," Opt. Express **19**(12), 11228–11235 (2011).
18. Y. Minami, K. Horiuchi, K. Masuda, J. Takeda, and I. Katayama, "Terahertz dielectric response of photoexcited carriers in Si revealed via single-shot optical-pump and terahertz-probe spectroscopy," Appl. Phys. Lett. **107**(17), 171104 (2015).
19. Z.-H. Zhai, S.-C. Zhong, J. Li, L.-G. Zhu, K. Meng, J. Li, Q. Liu, Q.-X. Peng, Z.-R. Li, and J.-H. Zhao, "Time-resolved single-shot terahertz time-domain spectroscopy for ultrafast irreversible processes," Rev. Sci. Instrum. **87**(9), 095101 (2016).
20. K. Y. Kim, B. Yellampalle, J. H. Glownia, A. J. Taylor, and G. Rodriguez, "Measurements of terahertz electrical conductivity of intense laser-heated dense aluminum plasmas," Phys. Rev. Lett. **100**(13), 135002 (2008).
21. G. T. Noe, I. Katayama, F. Katsutani, J. J. Allred, J. A. Horowitz, D. M. Sullivan, Q. Zhang, F. Sekiguchi, G. L. Woods, M. C. Hoffmann, H. Nojiri, J. Takeda, and J. Kono, "Single-shot terahertz time-domain spectroscopy in pulsed high magnetic fields," Opt. Express **24**(26), 30328–30337 (2016).
22. Y. Minami, Y. Hayashi, J. Takeda, and I. Katayama, "Single-shot measurement of a terahertz electric-field waveform using a reflective echelon mirror," Appl. Phys. Lett. **103**(5), 051103 (2013).
23. M. Walther, D. G. Cooke, C. Sherstan, M. Hajar, M. R. Freeman, and F. A. Hegmann, "Terahertz conductivity of thin gold films at the metal-insulator percolation transition," Phys. Rev. B **76**(12), 125408 (2007).
24. Z. Jiang, F. G. Sun, Q. Chen, and X.-C. Zhang, "Electro-optic sampling near zero optical transmission point," Appl. Phys. Lett. **74**(9), 1191–1193 (1999).
25. K.-J. Kim, K. T. McDonald, G. V. Stupakov, and M. S. Zolotorev, "Comment on "Coherent acceleration by subcycle laser pulses"," Phys. Rev. Lett. **84**(14), 3210 (2000).
26. C. A. Werley, Q. Wu, K.-H. Lin, C. R. Tait, A. Dorn, and K. A. Nelson, "Comparison of phase-sensitive imaging techniques for studying terahertz waves in structured $LiNbO_3$," J. Opt. Soc. Am. B **27**(11), 2350–2359 (2010).
27. F. Blanchard, A. Doi, T. Tanaka, H. Hirori, H. Tanaka, Y. Kadoya, and K. Tanaka, "Real-time terahertz near-field microscope," Opt. Express **19**(9), 8277–8284 (2011).
28. F. Blanchard, A. Doi, T. Tanaka, and K. Tanaka, "Real-Time , Subwavelength Terahertz Imaging," Annu. Rev. Mater. Res. **43**(July), 237–259 (2013).
29. P. C. M. Planken, H.-K. Nienhuys, H. J. Bakker, and T. Wenckebach, "Measurement and calculation of the orientation dependence of terahertz pulse detection in ZnTe," J. Opt. Soc. Am. B **18**(3), 313–317 (2001).
30. F. D. J. Brunner, J. A. Johnson, S. Grübel, A. Ferrer, S. L. Johnson, and T. Feurer, "Distortion-free enhancement of terahertz signals measured by electro-optic sampling I Theory," J. Opt. Soc. Am. B **31**(4), 904–910 (2014).
31. J. A. Johnson, F. D. J. Brunner, S. Grübel, A. Ferrer, S. L. Johnson, and T. Feurer, "Distortion-free enhancement of terahertz signals measured by electro-optic sampling II Experiments," J. Opt. Soc. Am. B **31**(5), 1035–1040 (2014).
32. M. Tinkham, "Energy gap interpretation of experiments on infrared transmission through superconducting films," Phys. Rev. **104**(3), 845–846 (1956).
33. A. J. Gatesman, R. H. Giles, and J. Waldman, "High-precision reflectometer for submillimeter wavelengths," J. Opt. Soc. Am. B **12**(2), 212–219 (1995).
34. N. Laman and D. Grischkowsky, "Terahertz conductivity of thin metal films," Appl. Phys. Lett. **93**(5), 051105 (2008).
35. N. Kaiser, "Review of the fundamentals of thin-film growth," Appl. Opt. **41**(16), 3053–3060 (2002).
36. M. V. Exter, C. Fattinger, and D. Grischkowsky, "Terahertz time-domain spectroscopy of water vapor," Opt. Lett. **14**(20), 1128–1130 (1989).

1. Introduction

Terahertz (THz) time-domain spectroscopy (THz-TDS) using pulsed THz radiation is a versatile tool for studying the properties of insulating and conducting materials [1–5]. Unlike many other spectroscopic techniques used in the visible or infrared regimes of the electromagnetic spectrum, THz-TDS relies on recording the THz time-domain waveform by essentially performing a pump-probe experiment to determine the THz-induced transient birefringence in an electro-optic (EO) crystal [6, 7]. Measuring the birefringence while varying the time delay between the THz pulse and the femtosecond readout pulse yields the THz time-domain electric field, $E(t)$, from which one can extract the complex-valued spectrum $\tilde{E}(\omega) = |E(\omega)| \exp(i\phi(\omega))$ by performing a numerical Fourier transform. Because the amplitude and phase of the field are obtained, this has the advantage that complex-valued material parameters (e.g. refractive index, $\tilde{n}(\omega) = n(\omega) + i\kappa(\omega)$ and conductivity, $\tilde{\sigma}(\omega) = \sigma'(\omega) + i\sigma''(\omega)$) can be evaluated from a

single transmission or reflection mode measurement without needing to invoke the Kramers-Kronig relations. By taking advantage of multi-shot averaging, the signal-to-noise ratio (SNR) of a THz-TDS measurements can exceed 10^4:1 when using an amplified laser system [8], or even 10^6:1 when using a high repetition rate oscillator based system [9], leading to sensitive and quantitative measurements. While THz-TDS has proven extremely successful, the multi-shot, scanning-based nature of THz-TDS is time-intensive, and studies of short-lived states of matter undergoing irreversible changes are impractical using conventional methods.

In order to overcome these issues, single-shot THz detection methods have been developed as a means for quickly and accurately measuring THz temporal waveforms [10]. These methods rely on the ability to capture a full THz waveform using a single temporally [11–13] or spatially [14–17] shaped readout pulse to sample the temporal profile of the THz field on a multi-element detector. Single-shot THz detection methods have been used to successfully measure the THz frequency static material properties of lactose [17], characterize radiation from electron bunches [12], and study the dynamics of photoexcited silicon [18, 19], laser heated dense plasmas [20], and silicon in strong magnetic fields [21]. Although these detection schemes have been referred to as “single-shot", they require at least two separate measurements to record a THz waveform: one with the THz induced change on the readout pulse, I, and one of the unperturbed readout pulse, I_0. These are used to determine the relative intensity change in the readout pulse, $\Delta I/I_0 = I/I_0 - 1$, which can be related to the THz field. However, as these measurements are not taken simultaneously, noise can be introduced from the shot-to-shot fluctuations. This can be particularly damaging for high-energy and low-repetition rate lasers, where multiple amplification stages, large size, and long path length often result in appreciable changes in both the beam pointing and the pulse energy. Furthermore, many of the single-shot experiments performed have still utilized averaging of single-shot traces to determine the THz time-domain waveform and spectrum, and variations in the THz pulse between signal and reference can affect the measurement.

Here, we present a self-referencing method for simultaneously collecting signal and reference waveforms in a single-shot by detecting multiple images and using a set of correlation functions to compensate the shot-to-shot fluctuations. To test the method, we use a single-shot technique based on a reflective 1D echelon [18, 21, 22]. The 1D echelon is a modified version of the 2D transmissive echelon demonstrated for THz spectroscopy by Kim *et. al* [16], and has the additional advantage that there is no loss of temporal resolution due to broadening of the pulse duration caused by material dispersion. In the manuscript by Minami *et. al.*, [22], a self-referencing approach was suggested to reduce the noise of the measurement. We quantified the root-mean-square error of this approach and compared it against conventional referencing and a polarization-based balancing scheme [10, 21]. Finally, we illustrated the utility of this method by experimentally determining the DC conductivity of a 30 nm free standing gold film by THz-TDS in a transmission geometry. This has been previously reported using conventional THz-TDS [23], and demonstrates the capability of the correlation function method for performing measurements which require a high SNR.

2. Experimental setup and methods

The setup used is shown schematically in Fig. 1. All the experiments were performed using a Ti:Sapphire laser system with a regenerative amplifier and second-stage multipass amplifier. This system delivers approximately 5.5 mJ pulses, centered at 800 nm, with a duration of 45 fs FWHM at a maximum repetition rate of 120 Hz. The repetition rate was lowered to 20 Hz using a Pockels cell and a polarizer. Approximately 3 mJ was split using a non-polarizing beam splitter and used to pump a 1 mm thick ZnTe crystal, which produced THz pulses through optical rectification. A polyethylene plate was placed immediately after the crystal to block any residual pump light while allowing the THz pulse to be transmitted. The THz pulse was then

focused using a 2 inch diameter, 2 inch effective-focal length off axis parabolic reflector onto the sample. This spot was then relay imaged onto a 1 mm thick ZnTe crystal for EO detection. Additionally, a 2 mm thick 20 kΩ cm silicon wafer was placed between the generation crystal and the first focusing parabolic reflector, and was used to direct a portion of the THz pulse to another ZnTe crystal. The waveform of this pulse was simultaneously measured and served as the reference.

The remaining laser pulse energy was used for single-shot EO sampling using a reflective stair-step echelon [22]. The echelon used in these measurements consisted of 500 gold coated steps which were 30 μm wide and 5 μm tall. This split the single incident pulse into 500 smaller pulses separated by a delay that is dependent on the step height and the incidence angle. In these experiments, the incidence angle was approximately 10°, corresponding to a time delay between pulses of $t \sim 33$ fs and and maximum time window of $T \sim 17$ ps. The time resolution, which was limited by the 100 μm spatial resolution of the imaging system, was 100 fs.

After setting the polarization of the readout pulse to vertical, the readout pulse was reflected off the echelon and then was split into three arms and used to detect (a) a THz waveform which probed the sample, in this case in transmission, (b) a THz waveform which did not encounter the sample, and (c) the unmodified probe which monitored the laser pointing and energy fluctuation. Readout pulses to probe waveforms (a) and (b) were focused through a hole in their respective off-axis parabolic reflectors using $f = 10$ cm lenses and overlapped with their appropriate THz pulses in 1 mm thick ZnTe crystal for EO detection of the THz fields. A second $f = 10$ cm lens placed after each ZnTe crystal was used to produce an image of the echelon on identical CCD

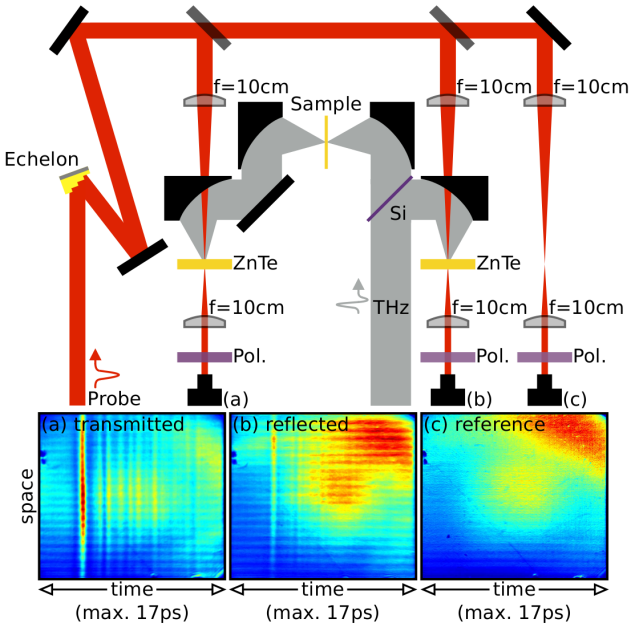

Fig. 1. Schematic illustration of the setup. The THz field was split into two arms – one probed the sample in transmission mode while the other served as a reference. The readout sampling beam was reflected off the echelon and split. Two of the arms measured (a) probing and (b) reference THz waveforms. The remaining arm (c) monitored shot-to-shot fluctuations. The horizontal stripes result from imperfections in the imaging system. Images (a), (b) and (c) are the raw images taken on a single shot by the 3 CCD cameras labeled (a), (b), and (c) in the schematic.

cameras (Allied Vision Manta G-201, 12-bit 30fps). Pulse (c) was also imaged onto a CCD camera using identical lenses, but no ZnTe was placed at the focus of the first lens. Representative images recorded with the modified and reference sampling pulses are shown in Figs. 1(a), and 1(b), and 1(c). The horizontal stripes in Figs. 1(a) and 1(b) come from imperfections in the imaging system and needing to image through the hole in the off-axis parabolic reflector. These stripes are also visible in Fig. 1(c), but are visible to a lesser degree because the beam was not imaged through a finite aperture.

For both of the methods, the THz waveforms were determined using two images – one where the THz pulse overlapped with echelon pulses, and one with the THz pulse absent. The former was divided by the latter to construct a ratio image in which the relative signal modulation, $\Delta I/I_0$, was related to the THz field amplitude. Due to the 1D structure of the echelon, the horizontal axis represents the time-delay in a conventional delay-stage measurements. The ratio images were averaged as $\Delta I/I_0$ was uniform along the vertical axis. In practice, we found it was necessary to apply linear perspective transformations on the images in either Python or MATLAB to correct for tilting before extracting the waveforms.

2.1. Correlation function-based approach

Our proposed self-referencing method used two types of correlation functions to extract and analyze the THz waveforms: image correlation functions and a spectral correlation function. For the transmitted and reflected THz pulses, the image correlation functions were determined by averaging the ratio images obtained with camera (a) or (b) as the "signal" and camera (c) as the "reference": $I_C^{a,b} = I_0^{a,b}/I_0^c$. This was then used to transform an image measured on camera (c) to the equivalent reference image on cameras (a) or (b):

$$\frac{\Delta I^{a,b}}{I_0} = \frac{I^{a,b}}{I_0^c I_C^{a,b}} - 1. \tag{1}$$

THz waveforms were measured by EO detection with a nearly crossed-polarizer ($\theta \sim 10^\circ$ deviation from crossed) placed after the ZnTe crystal. The THz field-induced birefrigence rotated the polarization of temporally overlapped echelon pulses resulting in a relative intensity change given by [24],

$$\frac{\Delta I^{a,b}}{I_0} = \frac{\sin^2(\Delta\phi/2 + \Gamma/2) - \sin^2(\Gamma/2)}{\eta + \sin^2(\Gamma/2)} \approx \frac{\frac{1}{2}(\Delta\phi)(\Gamma)}{\eta + \Gamma^2/4}, \tag{2}$$

where Γ and η are contributions to background light arising from the static, strain-induced birefringence of the ZnTe crystal and the misaligned polarizer, and

$$\Delta\phi = \frac{2\pi\ell}{\lambda} n^3 r_{41} E_0, \tag{3}$$

is the phase shift caused by the transient birefringence. Here E_0 is the THz electric field, ℓ is the thickness of the ZnTe, n is the refractive index of the ZnTe at 800 nm, and r_{41} is the EO coefficient of the ZnTe. THz traces were extracted from ratio images by averaging along the vertical axis. Note that $\Delta I^{a,b}/I_0$ behaves linearly only in the limit of small THz fields. To verify linearity of our detection scheme, we measured the mean value of the time-domain THz waveform without any sample. We found that this value was on the order of the minimum detectable signal limit of our measurement with no base line offset. Because the THz waveform should integrate to zero [25], this is a good indication that our measurement was within the linear regime. For sufficiently large signals, contributions from the non-linear dependence on the signal on $\Delta\phi$ have a non-negligible effect on the waveform recorded [24], and the average the waveform differs significantly from zero. This is important for spectroscopic applications as it affects the spectrum measured when the sample is present compared to when it is absent.

The effect of the image correlation functions can be seen by comparing Figs. 2(a) and 2(c), which measure 5 raw single-shot THz waveforms transmitted through a 30 nm gold film before and after the correction by image correlation function, or Figs. 2(b) and 2(d), which report fields reflected off the silicon wafer. Traces with matching colors are derived from the same laser pulse. In this case, the image correlation function was constructed by averaging 20 images of the echelon with the THz pulse blocked. The large variations in Figs. 2(a) and 2(b) result from the shot-to-shot fluctuation of the laser pulses that illuminated the echelon. After applying the image correlation function, all the traces are well overlaid on each other as shown in Fig. 2(d). The improvement is much more prominent between Figs. 2(a) and 2(c) because only a small portion of the THz pulse is transmitted through the film, and the peak amplitude is on the order of the minimum detectable signal. This demonstrates that by using the image correlation functions to determine a reference image on the same laser pulse as the signal image significantly reduces distortions in the image which arise from shot-to-shot fluctuations, enabling measurements with low SNR.

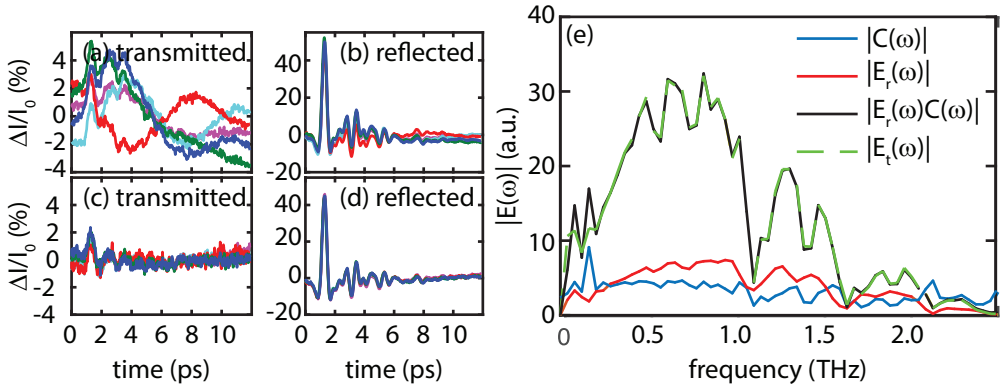

Fig. 2. Five individual single-shot THz waveforms obtained from a THz field: (a), (c), transmitted through a 30 nm gold film, and (b),(d) reflected using a silicon wafer. In (a) and (b) I_0 was measured at a much later time, while (c) and (d) used the image correlation functions to estimate I_0. The mean of the traces were subtracted to center them around 0. The same color THz waveforms in (a) and (b) were taken in a same shot. (e) Test of the spectral correlation function. The green dashed line is the experimentally measured transmitted THz ($|E_t(\omega)|$) from a single shot spectrum; the red line is the reflected THz spectrum ($|E_r(\omega)|$) measured from the same shot and the blue line is the correlation function ($|C(\omega)|$) between the transmitted and reflected THz; the black line is the product of $|E_r(\omega)|$ and $|C(\omega)|$.

Next, the spectral correlation function, $\tilde{C}(\omega)$, was determined using simultaneously measured THz transmission $\tilde{E}_T(\omega)$ and reference spectra $\tilde{E}_R(\omega)$. These were obtained by Fourier transformation of the time-domain waveforms. The spectral correlation function, $\tilde{C}(\omega)$, was then calculated from the average ratio of the transmitted spectrum to the reflected spectrum:

$$\tilde{C}(\omega) = \tilde{E}_T(\omega)/\tilde{E}_R(\omega). \tag{4}$$

To demonstrate the robustness of this approach, 20 single-shot measurements were first taken to construct a spectral correlation function with no sample present. This was then tested by taking individual single-shot measurements and calculating the spectrum of the transmitted THz waveform based on the measured reflected waveform from the same shot. Figure 2(e) shows the result, where the measured transmission spectrum from one single-shot measurement is shown in the green dashed line, and the calculated transmission spectrum is shown in the black

solid line, using the measured reflected THz (red line) and correlation function (blue line). The excellent agreement between the traces illustrates the utility of the spectral correlation function.

In practice, we found that the correlation functions are most effective when calibrations are recorded shortly before carrying out the actual measurements. This most accurately compensates for the long term drift of conditions such as of beam pointing, beam profile variation, and the overlapping between the sampling pulse and the THz beam in the EO sampling crystal. Although the correlation functions were stable within a day, we found that the correlation functions needed to be tested at least once per day to ensure proper corrections.

2.2. *Polarization-gated balancing*

In order to benchmark our approach, we compared the noise performance of the self-referencing scheme to the state-of-the-art polarization-gated balancing scheme. Polarization-gated balancing is typically used in THz-TDS and has also been successfully adapted for near-field THz imaging [26–28] and single-shot methods using echelons [10, 21]. Here, a quarter-waveplate with its fast axis rotated 45° from vertical and a Wollaston prism set to transmit *s*-(+) polarized and *p*-(-) polarized pulses were placed after the ZnTe crystal used for EO detection. Using a small splitting (3°) angle Wollaston allowed us to capture both polarization states on a single CCD camera. Images were recorded with the THz pulse present, $I^{\pm}$, and absent, $I_0^{\pm}$. The relative intensity change for this arrangement is given by [29]

$$\frac{\Delta I^{\pm}}{I_0^{\pm}} = \frac{I^{\pm}}{I_0^{\pm}} - 1 = \pm \sin(\Delta\phi). \tag{5}$$

This is equivalent to equation 2 but with $\Gamma = \pm\pi/2$ and $\eta = 0$. Compared to the self-referencing method, the measured signal can always be made linearly proportional to the applied field.

Figure 3(a) and 3(b) show the ratio images and the extracted THz waveforms for the *s*- and *p*-polarizations. Balancing is implemented by taking advantage of the fact that the waveforms

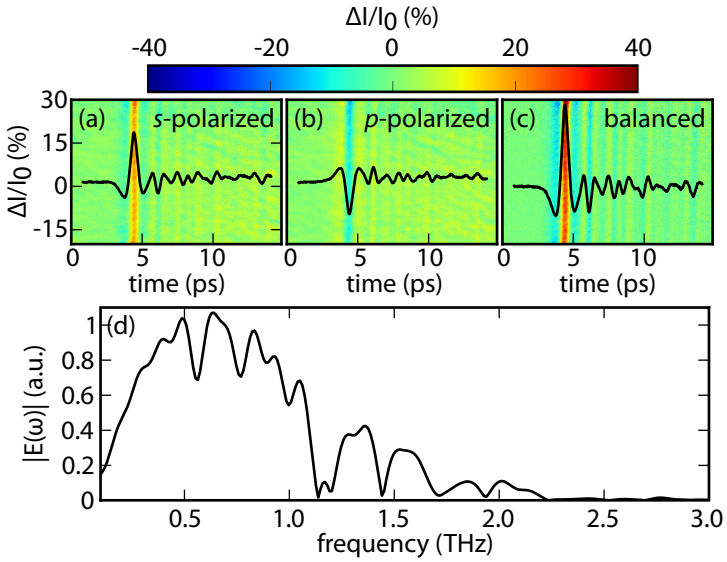

Fig. 3. Echelon ratio images and extracted THz waveforms for (a)*s*-polarized and (b) *p*-polarized images. The sign of the THz field is opposite between the two cases. (c) Polarization balanced echelon image and corresponding THz waveform. (d) Spectrum of balanced THz waveform.

recorded in the different polarization states have opposite sign from each other. Since fluctuations that arise due to power or pointing instabilities have the same sign, subtracting the waveforms from the two polarizations reduces noise while also doubling the signal. In this case, the images were put into register by taking a 2D cross-correlation. The result of the balancing procedure is demonstrated in Fig. 3(c), where there is a clear doubling of the signal amplitude and the images and traces are centered around $\Delta I/I_0 = 0$.

3. Noise comparison

In order to evaluate the noise performance of the self-referencing method, time-domain waveforms were measured with the the THz pulses blocked. The results give a measure of variations arising due to noise in the electronics which cannot be compensated.

Representative results are shown in Fig. 4. Figure 4(a) serves as a baseline and presents a trace obtained using "signal" and "reference" readout pulses measured at different times. Figures 4(b) and 4(c) correspond to traces extracted using the correlation function when the readout pulse measured on the "signal" camera is attenuated to low [Fig. 4(b)] or high [Fig. 4(c)] levels. Finally, Fig. 4(d) gives the results for the polarization balanced case.

In order to quantify the noise, the root-mean-square (RMS) deviation was measured for 20 single-shot traces. The average and the standard deviation in the RMS for the four cases are shown in the bottom right corner of each figure. The data indicate that polarization-gated balancing provides the lowest noise floor, and has the smallest variation in the RMS. This can be understood by realizing that the correlation function based approach essentially uses a cross-correlation between related images to remove structure in the image and thereby increase accuracy and reduce noise. When the images are highly correlated, as in the high-light case where there is little structure in the correlation function, the noise suppression is effective. In the low-light case, the correlation is weak and this raises the noise floor. These both have a smaller deviation in RMS compared to not using a correlation function, indicating the effect of referencing with the same laser pulse. In comparison, polarization-gated balancing essentially uses an autocorrelation between identical images to remove correlated noise while also amplifying the signal. Because this correlation is always strong, polarization gated balancing routinely produces the lowest noise floor.

It is worth noting that there are still advantages to this self-referencing scheme. In cases where there is an isotropic change (for example, optical reflectivity measurements, stimulated emission experiments, or certain stimulated scattering experiments) the signal modulation will not show a polarization dependent response. In these instances, balancing by subtracting orthogonal polarizations will remove the signal. Additionally, for polarization sensitive measurements it is possible to tune the polarizer angle to optimize the signal modulation and compensate for the increased noise expected in the self-referencing method [24, 30, 31]. This can be useful if the signal amplitude is very small, or when the THz field is consistently small.

4. Single-shot measurements on 30 nm gold film

Finally, in order to demonstrate the capabilities of these techniques for measuring small signals, we measured the conductivity of a 30 nm free-standing gold film. The free-standing film was fabricated by first depositing gold on a very thin layer of soap (LiquiNox concentrated soap) coated on glass substrate surface using a DC magnetron sputtering machine at room temperature. The film was subsequently lifted off by using distill water to dissolve the soap layer. The free-standing film was mounted on a sample card with holes of 2 mm diameter, and they were inspected to be pinhole-free using a backlit imaging system with sub 10 μm resolution before the THz transmissivity measurement. Some of the lifted off films were mounted smoothly on a clean glass surface for thickness calibration using an atomic force microscope, and conductivity measurement by 4-point probe, a standard method to measure thin film DC conductivity. Using

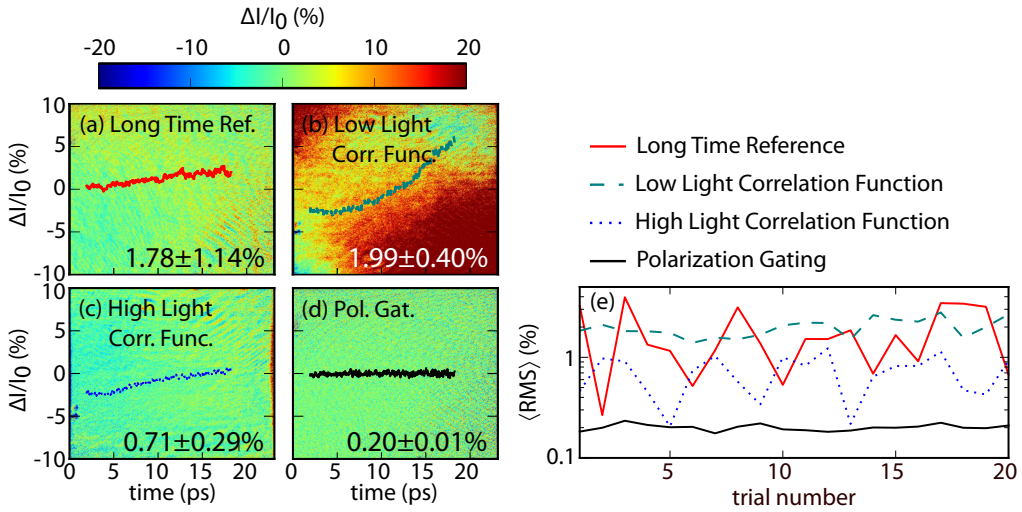

Fig. 4. Images and time traces illustrating the noise performance when referencing with a reference pulse measured (a) at a different time, (b)/(c) at the same time and corrected using a correlation function, and (d) at a different time and corrected using polarization gated balancing. The values in the lower right corner of each image are the average and standard deviation of the RMS deviation over 20 measurements. (e) Plot of the average RMS deviation of the 20 noise traces in the four different cases.

20 single-shot measurements, the complex-transmission coefficient, $\tilde{t}(\omega)$, was determined and related to the complex conductivity according to the the Tinkham equation [32]:

$$\tilde{\sigma}(\omega) = \frac{2}{Z_0 d}\left(\frac{1}{\tilde{t}(\omega)} - 1\right), \tag{6}$$

where $Z_0 = 377\ \mathrm{S}^{-1}$ is the impedance of free space and d is the thickness of the film.

The result is shown in Fig. 5, along with the measured DC conductivity of gold found using a 4-point probe. These results were compared against the Drude model,

$$\sigma(\omega) = \frac{\sigma_0}{1 - i\omega\tau}, \tag{7}$$

where the σ_0 is the DC conductivity, and τ is the carrier scattering time. For gold, the inverse of the scattering time is much larger than the highest frequency in the THz bandwidth ($1/\tau \sim$ 30 THz), so $\sigma(\omega) \approx \sigma_0$. In these measurements, the average conductivity from 0.7 to 1.0 THz was $(1.3 \pm 0.4) \times 10^7$ S m^{-1} for the correlation function approach and $(1.2 \pm 0.4) \times 10^7$ S m^{-1} for polarization gated balancing. These values are in good agreement with the the value of $(1.68 \pm 0.13) \times 10^7$ S m^{-1} found using the 4-point probe. The significantly lower conductivity compared to the bulk value [33] was also observed in 28 nm [23], 85 nm, and 150 nm [34] gold thin films deposited on silicon substrates. This can be ascribed to the intrinsic defects associated with the growth of nanocrystalline film, which are expected to play a significant role in limiting the conductivity [35]. In comparison against the data collected with polarization gating method, there is good agreement between 0.8 to 1.0 THz. We believe that the discrepancies in the data come from contamination absorption by water vapor in the experimental setup. In particular, the strong absorption lines at 0.75 THz and 1.1 THz [36] dominate the otherwise small imaginary component of the conductivity. This leads to the large amplitude of σ'' near those frequencies, in particular the anomalously negative values. In addition, as the experiments were performed on different days, change in the temperature or humidity result in differences in the strength of

the water absorption. This can be dealt with systematically by purging the system with dry air, which removes the water absorption.

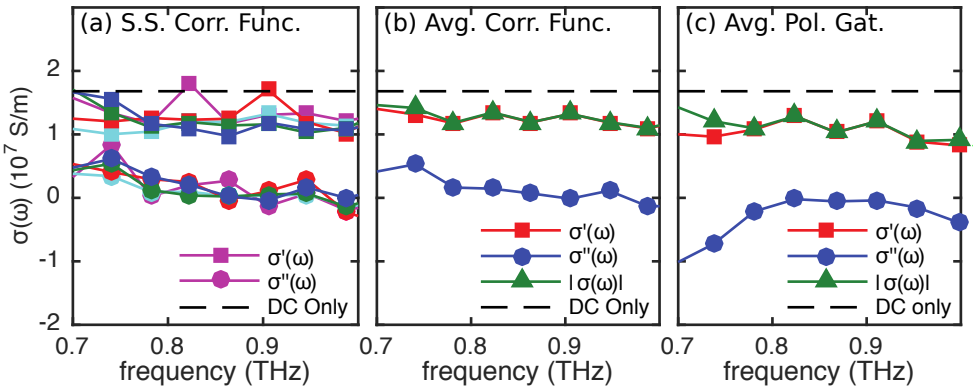

Fig. 5. Conductivity of 30nm freestanding Au measured using 4-point probe and single shot THz detection using the correlation function and polarization gated balancing schemes. The dashed line is the conductivity measured by four-point-probe. (a) 5 single-shot conductivity measurements using a correlation function with colors corresponding to the same shots in Fig.2. (b) and (c) show the average of 20 measurements using a correlation and polarization-gated balancing respectively. $\sigma'(\omega)$ and $\sigma''(\omega)$ are the real and imaginary parts of the THz conductivity, $|\sigma(\omega)|$ is the corresponding absolute value, and "DC only" represents the valued measured by 4-point probe.

5. Conclusion and outlook

In conclusion, we have demonstrated a balancing scheme capable of self-referencing in single-shot THz-TDS measurements. Fluctuations of the sampling pulse and the THz pulse are monitored on each shot. This method is able to provide all the information needed for the measurement once the proper correlation functions are constructed with comparable SNR to the polarization-based balancing scheme. We have compared the noise floor of this method against a polarization-gated balancing scheme and found that the two have comparable noise performance. Lastly, we utilized the correlation function to measure the conductivity of a 30 nm gold thin-film using a true single-shot THz technique, and found good agreement with an independent measurement of the DC conductivity by 4-point probe.

To further optimize of the self-referenced single-shot THz scheme, the polarization gated balancing should be applied to both the THz sampling and reference arms to lower their overall noise floor. Also improving the THz generation and detection efficiency by using thicker ZnTe crystals will improve the THz field strength and hence improve the SNR. The imaging of the echelon can also be improved by using a pellicle beamsplitter to overlap the readout pulses with the echelon. This would also allow for the use of a longer focal length lens and reduce aberrations resulting from clipping by the hole in the parabolic mirror.

Understanding the limitations of single-shot THz techniques is important for their successful implementation in other experiments. In future studies probing structural or electronic phase transitions, or short lived states of material under extreme conditions, such as warm dense matter, having accurate low-noise diagnostics is essential for obtaining accurate results. Furthermore, the concepts applied here for understanding noise reduction schemes are important for many single-shot techniques.

Funding

This study was supported by DOE Office of Science, Fusion Energy Science under FWP 100182 and Natural Sciences and Engineering Research Council of Canada.